PCCP

Accepted Manuscript

ROYAL SOCIETY OF CHEMISTRY

www.rsc.org/pccp

Journal Name

RSCPublishing

ARTICLE

Cyclopenta[1,2-b:5,4-b′]dithiophene-Porphyrin Conjugate for Mesoscopic Solar Cells: A D-π-D-A Approach

Cite this: DOI: 10.1039/xoxxoooooox

Received ooth January 2012,
Accepted ooth January 2012

DOI: 10.1039/xoxxoooooox

www.rsc.org/

Jianfeng Lu,[a] Bingyan Zhang,[a] Shuangshuang Liu,[a] Hao Li,[a] Huailiang Yuan,[a] Yan Shen,*[a] Jie Xu,*[b] Yibing Cheng[a,c] and Mingkui Wang*[a]

In this article, cyclopenta[1,2–b:5,4–b′]dithiophene (CPDT) was introduced as spacer between porphyrin chromophore and cyanoacetic acid to obtain a porphyrin dye (coded as LW9). The resulted novel porphyrin dye exhibits an extended absorption spectra and a split B band at 520 nm. Therefore, a full spectrum light harvesting characterization of sensitized TiO_2 mesoporous film can be achieved. To make a thoroughly investigation on the influence of spacer unit, new sensitizers conjugated with biphenyl (LW7) and bithiophene (LW8) have been synthesized. As the electron-donating ability of the spacer from biphenyl to bithiophene and cyclopenta[1,2–b:5,4-b′]dithiophene, stepwise red-shifted electronic absorption spectra and consistently decreased energy gap of the dye are presented. Evaluating these novel porphyrin with dye sensitized solar cell, power conversion efficiency of 6.5% is achieved employing $[Co(bpy)_3]^{2+/3+}$ redox couple for LW9 device under reporting conditions. Detailed investigation, including time-resolved photoluminescence, transient photovoltage decay, and scanning electrochemical spectroscopy measurements, provides important information on the factors affecting the principal photovoltaic parameters. The present report highlights the potential of D–π–D–A porphyrin for development of efficient sensitizers with broadly light absorption property.

Introduction

Dye-sensitized solar cells (DSSCs) have attracted growing interests due to their high indoor power conversion efficiency and low cost compared to inorganic solar cells.[1] In the last 20 years, DSSCs using ruthenium(II)–based sensitizers have reached overall solar-to-electric power-conversion efficiency (PCE) of 11.4 % under full sun illumination (AM 1.5G, 1,000 W m^{-2}).[2] As ruthenium is a noble and expensive metal, the research activity has increased in exploring ruthenium-free sensitizers.[3] Porphyrin has been considered as one of the most promising candidates because of the up to near-infrared region electronic absorption spectra, long–lived π* singlet excited states for hot electron injection and tunable electrochemical and photophysical properties.[4] In this case, new benchmark in DSSCs with overall PCE of 13.0% was achieved by a donor-π-acceptor (D–π–A) porphyrin (SM315) with cobalt redox couple.[5]

In 2011, Lin and Diau *et al* reported a series of highly efficient porphyrin dyes, utilizing dialkylamine as donor in conjunction with ethynylbenzoic acid as acceptor. These dyes showed superior photovoltaic performance over 10%.[4a, 4b] As we know, elongation of the π conjugation and loss of symmetry in porphyrins cause broadening and a red shift of the absorption bands.[8] In this case, oligomer thiophenes,[9] 2,3,5,6–tetrafluorophenyl,[10] N–annulated perylene,[7, 11] anthracene,[12] and other functional groups[13] were successfully utilized to construct the porphyrins dyes. DSSC devices based on these sensitizers showed PCEs in the range of 4%~10.5%.[9-13] However, it is worth to note that few porphyrins simultaneous present strong light harvesting ability across from visible to near-IR region.[6c, 14] Recently, 2,1,3–benzothiadiazole (BTD) was introduced as linker between benzoic acid and porphyrin chromophore, affording porphyrins with filled valley between the B and Q bands.[5b, 6a] The device efficiency of GY50 and SM315 porphyrins were obviously increased due to the introduction of an electron–deficient group.[6a]

Inspired by Lin and Diau's pioneer work, electron-rich hetero-aromatics such as thiophene and 2,3–dihydrothieno[3,4–b][1,4] dioxine (EDOT) were introduced as π spacer between porphyrin macrocycle and cyanoacetic acid anchoring group by our group, aiming to extend light harvesting area into near–IR region.[15] As expected, these dyes with a thiophene or EDOT as spacer showed extended incident photon to current conversion efficiency (IPCE) up to 850 nm, demonstrating that electron-rich spacers were beneficial for intramolecular charge transfer in D–π–A porphyrins.[15] Along this track, cyclopenta[1,2–b:5,4–b′]dithiophene (CPDT) was introduced as spacer between cyanoacetic acid and porphyrin chromophore (LW9 dye) in this article. As we know, CPDT possesses strong electron–donating

ability comparing with thiophene or EDOT, as well as the steric effect of alkyl groups placed in the 4,4–position.[16] It was observed that the absorption valley between the B and Q–band was filled by a B band split at 520 nm, and the absorption bands were obviously broadened and red–shifted. As a result, LW9 dye exhibits strong light-harvesting character across from visible to near–IR region. To fully investigate the influence of the spacer on spectroscopic and photoelectric properties of the dyes, biphenyl and bithiophene conjugated porphyrins (coded as LW7 and LW8) were also synthesized. As the electron–donating ability of the spacer varied from biphenyl to bithiophene and CPDT, stepwise red–shifted absorption spectra and consistent decreased energy gap can be observed. We evaluated these dyes in DSSCs. To avoid the loss of photovoltage using iodide/triiodide electrolyte, in this study, $[Co(bpy)_3]^{2+/3+}$ redox couple (molecular structure see Scheme 1) were employed to improve the photovoltage as well as the efficiency of the DSSC devices. PCE of 6.5% was achieved with $[Co(bpy)_3]^{3+/2+}$ redox couple for LW9 device under reporting conditions. While for LW7 and LW8, it was 6.02% and 6.32%, respectively. Detailed investigation, including time–resolved photoluminescence, transient photovoltage decay, and scanning electrochemical spectroscopy measurements, provides important information on the spacer factors affecting the principal photovoltaic parameters.

Experimental section

Materials and synthesis. The structures and purity of all intermediates and final compounds (LW7, LW8, and LW9) were identified by NMR and mass spectrometry (see Supporting Information, Fig. S1–Fig. S7). For comparison, the LD14 sensitizer was also synthesized according to the literature.[4a]

Computational. The Frontier molecular orbitals for LW7-LW9 dyes were calculated via the density functional theory (DFT) method in DCM at the B3LYP/LANL2DZ with the Gaussian 03 package. Four step computational protocol strategies were used to determine the charge transfer features of rod-like porphyrin dyes efficiently. It aims to evaluate the distance separating the barycentre of the electron density gain/depletion upon electron transition. Through the Polarizable Continuum Model (PCM), all calculations in our case systematically considered the bulk solvent effects. Four dodecyloxy chains have been replaced by methyl groups in order to lighten the computational burden.

Device fabrication. FTO glass plates (3 mm thickness, 7Ω/square, Nippon Sheet Glass) were cleaned in detergent solution using the ultrasonic bath for 15 min and then rinsed with de-ionized water and ethanol for 15 min. A 7.5 μm thick transparent layer of 20 nm TiO_2 particles was first printed on FTO glass and then coated with a 5 μm thick second layer of 400 nm light scattering anatase particles (WER2–O, Dyesol). The film thickness was measured by DEKTAK (VECCO, Bruker). After treated with 40 mM aqueous $TiCl_4$ at 70 ^oC for 30 min, the TiO_2 film was first sintered at 500 ^oC for 30 min and then cooled to about 80 ^oC in air. The details for the preparation of the 20 nm TiO_2 particles and TiO_2 films have been described elsewhere.[2a] Then the TiO_2 film electrodes were dipped into a 200 μM dye solution in a mixture of toluene and ethanol (volume ratio, 1:1) at room temperature for 5 h. After being washed with ethanol and dried by air flow, the sensitized titania electrodes were assembled with thermally platinized conductive glass electrodes. The working and counter electrodes were separated by a 25 μm thick hot melt ring (Surlyn, DuPont) and sealed by heating. The internal space was filled with liquid electrolytes using a vacuum back filling system. The cobalt based electrolyte (coded W30) for devices was 0.165 M $Co(bpy)_3(PF_6)_2$, 0.045 M $Co(bpy)_3(PF_6)_3$, 0.8 M 4–tert–butylpiridine and 0.1 M $LiClO_4$ in acetonitrile. The devices were optimized with chenodeoxycholic acid (CDCA) as the coadsorbent with the optimized dye/CDCA ratio of 1:10.

Photovoltaic characterization A 450 W xenon light source solar simulator (Oriel, model 9119) with AM 1.5G filter (Oriel, model 91192) was used to give various irradiance at the surface of the solar cell. The current-voltage characteristics of the cell under these conditions were obtained by applying external potential bias to the cell and measuring the generated photocurrent with a Keithley model 2400 digital source meter (Keithley, USA). IPCE spectra were recorded with a Keithley 2400 Source meter (Keithley) as a function of wavelength under a constant white light bias of approximately 1 mW cm^{-2} supplied by a white LED array (IQE-LIGHT-BIAS, Newport). A 300 W xenon lamp (Oriel Co.) was used as the excitation beam source in combination with a Corstoner 260 monochromator (Newport) and chopped at 10 Hz. The devices with the photoanode area of 0.16 cm^2 were tested with a metal mask of 0.09 cm^2. The photovoltaic parameters were obtained by measuring a number of independently samples individuals.

Scanning Electrochemical Microscopy (SECM) Characterization SECM experiments were performed on CHI 920C electrochemical workstation (CH Instruments, Shanghai). A homemade Teflon cell (with volume of 2 mL) was used to hold a Pt wire counter electrode, an Ag/Ag^+ reference electrode. The photoanodes FTO/TiO_2/porphyrins sample films were attached to the cell bottom and sealed with an O–ring as work electrode. In SECM measurements, the dye-sensitized transparent semiconductor nanocrystal films (TiO_2 with a thickness of about 2.3 μm) were used as the working electrode. An extra Pt wire was connected to FTO substrate with the electrolyte in order to operate the photoelectrochemical cell in a short-circuit setup. A 25 μm diameter Pt wire (Goodfellow, Cambridge, UK) was sealed into a 5 cm glass capillary prepared by a Vertical pull pin instrument (PC–10, Japan). The ultra–microelectrode (UME) was polished by a grinding instrument (EG–400, Japan) and micro-polishing cloth with 1.0, 0.3 and 0.05 μm alumina powder. Then the UME was sharpened conically to a RG of 10, where RG is the ratio between the diameters of the glass sheath and the Pt disk. All experiments were carried out at room temperature. The irradiation was focused onto the backside of the photoanode from light emitting diode (red, Lumileds Lighting, USA).

Time-resolved photoluminescence (TRPL) experiment TPRL measurements were recorded with Edinburgh instruments (FLSP920 spectrometers). The excitation light source was a picosecond pulsed light-emitting diodes centered at 445 nm (10 ps pulses), operated at a frequency of 10 MHz. The TiO_2 nanoparticles were screen-printed on quartz substrates. The substrates coated with nanoparticles were immersed 200 μM dye solution, followed by rinsing and drying to remove the excess dye. Data fitting procedures was according to the literature,[24] Data collected for solution and TiO_2 samples were fitted by the convolution of the Gaussian instrument response function

with a single stretched exponential: Int = $A_0 e^{-(\tau/t)^{\beta}}$, where β is the stretch parameter. We set the β as 1 to obtain the excited singlet state Fluorescence lifetime of the samples.

Transient photovoltage decay (TPD) measurement The determination of the interfacial charge recombination lifetime was performed by transient photovoltage decay measurements and charge extraction experiments. For the transient decay measurements, a white–light bias was generated from an array of diodes. Blue–light–pulse diodes (0.05 s square pulse–width, 100 ns rise and fall time) that were controlled by a fast solid-state switch were used as the perturbation source. The voltage dynamics were recorded on a PC–interfaced Keithley 2602A source meter with a 500 ms response time. The perturbation light source was set to a suitably low level for the voltage-decay kinetics to be mono-exponential. By varying the intensity of white-light bias, the recombination lifetime could be estimated over a range of open-circuit voltages. The chemical capacitance of the TiO_2/electrolyte interface and the density of state (DOS) at V_{OC} were calculated according to Cμ=ΔQ/ΔV, where ΔV is the peak of the photovoltage transient and ΔQ is the number of electrons injected during the red-light flash. The latter parameter was obtained by integrating a short circuit transient photocurrent that was generated from an identical red-light pulse. Before the LEDs switched to the next light intensity, a charge-extraction routine was executed to measure the electron density in the film. In the charge-extraction techniques, the LED illumination source was turned off within <1 μs, whilst the cell was simultaneously switched from open circuit to short circuit. The resulting current, as the cell returned to V = 0 and J = 0, was integrated to give a direct measurement of the excess charge in the film at that V_{OC} value.

Results and Discussion

Synthetic procedures

The molecular structures of LW7, LW8, and LW9 sensitizers are presented in Scheme 1. Detailed synthetic procedure and compound characterizations are described in the supporting information. Briefly, standard Sonogashira cross–coupling reaction reported by Lindsey and co-workers were used to prepare LW7, LW8, and LW9 sensitizers (see Scheme S1).[17] The synthesis started with the key precursor 5–bromo–15–(4–N,N–dimethylamino-phenyl)ethynyl–10,20–bis[2,6–di(dodecyloxy)phenyl] porphinato zinc(II) (coded as Por–1) according to the literature.[18] Firstly, the π–spacer aldehydes (ethyl 4'–bromo–(1,1'–biphenyl)–4–carbaldehyde (compound **1**), 5'–bromo–(2,2'–bithiophene)–5–carbaldehyde (compound **2**), and 6–bromo–4,4–didodecyl–4H–cyclopenta[1,2–b:5,4–b'] dithio-phene–2–carbaldehyde (compound **3**) were coupled with trimethylsilylacetylene via Pd–catalyzed Sonogashira-coupling to obtain intermediates 4'–[(trimethylsilyl)ethynyl]–(1,1'–biphenyl)–4–carbaldehyde (compound **4**), 5'-[(trimethylsilyl) ethynyl] –(2,2'–bithiophene)–5–carbaldehyde (compound **5**), and 4,4–didodecyl–6–[(trimethylsilyl)ethynyl]–4H–cyclopenta[1,2–b:5,4–b']dithiophene-2-carbaldehyde (compound **6**). Then, 4'–ethynyl–(1,1'–biphenyl) –4–carbaldehyde (compound **7**), 5'–ethynyl–(2,2'–bithiophene)–5–carbaldehyde (compound **8**), and 4,4–didodecyl–6–ethynyl–4H–cyclopenta[1,2–b:5,4–b']dithiophene-2–carbaldehyde (compound **9**) were achieved by de-protection of trimethylsilyl with potassium carbonate. Compound Por–1 was coupled with the intermediate π–spacer aldehydes (compounds **7**, **8**, and **9**) through Sonogashira coupling reaction, affording the porphyrin aldehyde precursors (compounds **10**, **11**, and **12**), whose molecular structures are illustrated in scheme S1. The target porphyrins LW7, LW8, and LW9 were achieved by Knoevenagel condensation with cyanoacetic acid and piperidine. The structure and purity of all reactive intermediates and final compounds were identified by NMR and mass spectroscopy (see supporting information Fig. S1–S7).

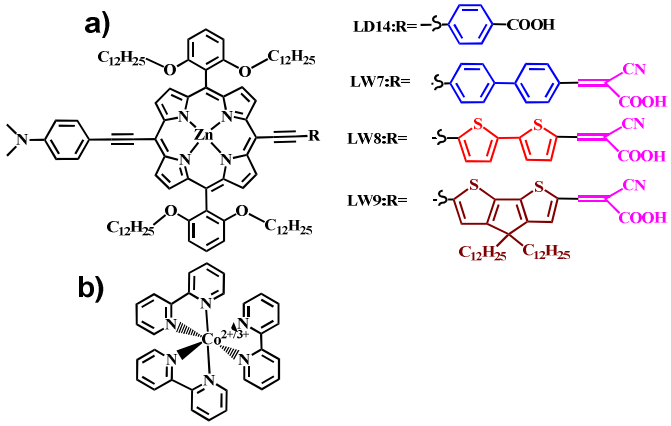

Scheme 1. a) Molecular structure of porphyrin sensitizers LW7, LW8, and LW9. LD14 is model sensitizer for comparison; b) Structure of the cobalt-complex redox couple.

Photophysical Properties

Fig. 1 presents the absorption spectra of LW7, LW8, LW9, and LD14 sensitizers in THF solution and the corresponding data are tabulated in Table 1. In solution, LW7, LW8, and LW9 sensitizers exhibited progressive red-shifted and broadened absorption spectra. The absorption peaks in visible region were found at 461, 467, and 471 nm for the B band, 670, 684 and 697 nm for the Q band, stemming from $S_0 \rightarrow S_2$ transition and $S_0 \rightarrow S_1$ transition, respectively.[19] Comparing to the LD14 dye (with D–π–A structure), LW8 (with D–π–π–A structure) and LW9 dye (with D–π–D–A structure) showed higher molar extinction coefficient (about 8×10^4 M^{-1} cm^{-1}) in the range of 650-750 nm. Thus, a strong near-IR light-harvesting ability was expected of the porphyrin sensitized TiO_2 film, which could lead an improvement of J_{SC} upon sensitization.[20] The LW8 absorption spectra was entirely red–shifted comparing to the LW7 dye (with biphenyl), indicating that bithiophene is more beneficial for extending the absorption spectra than biphenyl in this system. The bathochromic shift observed in the LW8 dye compared to LW7 may due to the more efficient intramolecular charge transfer transition. This may be caused by the change of electron-donating ability of bithiophene spacer moiety. The phenomenon is even clear when bithiophene in the LW8 was switched to CPDT in the LW9 dye, presenting extended absorption spectra and a obvious shoulder at 520 nm. This is helpful for filling the light–harvesting valley in the range of 500-600 nm comparing with conventional porphyrin sensitizers. Fig. S8 presents absorption spectroscopy of LW9-stained 2.3 μm TiO_2 film, showing the obvious shoulder at 520 nm and significant broadened absorption spectra. The peak of the LW9's Q band was red–shifted 14 nm relative to LW8, suggesting an efficient intra–molecular charge transfer behaviour. As we know, elongation of π conjugation and loss of symmetry in porphyrins are two of main strategies for

broadening the light-harvesting area of porphyrin dyes.[8c] The two thiophene groups in LW8 dyes are free to rotate. The conjugation would be broken if the two thiophene are not co-planar. While for LW9 dye, the conjugation across the rigid structure of CPDT group was more efficient. Thus, it was suggest that the difference of the absorption spectra should be attributed to the elongated conjugation in the LW9 dye. The stepwise red–shifted absorption spectra of LW7, LW8, and LW9 were consistent with the trend of their fluorescence emission spectra (Fig. S9). The maximum fluorescent emission bands of LW7, LW8, and LW9 porphyrins were found at 686, 702, and 725 nm, showing mirror images of their Q bands. The same trend suggested that the variety spacer units similarly affect push–pull porphyrin in photon absorption and emission.

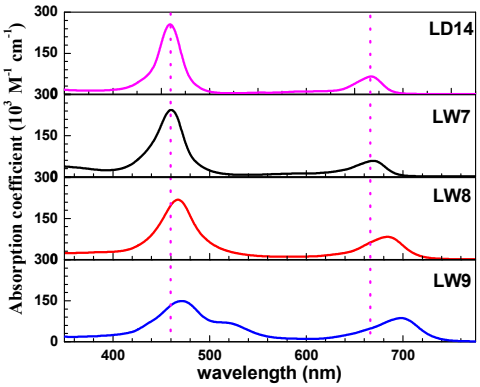

Fig. 1 UV–vis absorption spectroscopy measurement of the LW7, LW8, and LW9, and LD14 porphyrins in THF.

Electrochemical Properties

The electrochemical behaviour of new sensitizers was explored with cyclic voltammetry. The results are presented in Fig. S11 and Table 1. The first oxidation potential (Eox) of LW7, LW8, and LW9 dyes were estimated to be 0.70, 0.72, and 0.73 V, respectively, which were higher than that of $[Co(bpy)_3]^{2+/3+}$ redox couple (≈0.57 V vs. NHE).[21] According to the literature,[5g] the first oxidations are assigned to the porphyrin ring oxidation and the second assigned to the dimethylaminophenyl group, respectively. Thus, the very similar oxidation and reduction behaviours could be explained by the identical structure of the donor and porphyrin group in our case. The very small variation in the oxidation potentials may be due to the different spacer groups. The HOMO–LUMO gaps were determined to be 1.83, 1.79, and 1.75 eV for LW7, LW8, and LW9 sensitizers by intersection of the normalized absorption and emission spectrum. Thus, the dye excited state (dye^+/dye^*) were calculated to be –1.13, –1.07 and –1.01 V (vs. NHE), respectively. Fig. S11 presents the energetic alignment of S^0 and S* energy levels of the three porphyrins with the conduction band of TiO_2 and the redox potential of $[Co(bpy)_3]^{2+/3+}$ electrolyte, showing an effective electron injection is energetically possible from the excited dye to the TiO_2.

Computational

Density functional theory (DFT) at the B3LYP/6-31G level was used to gain the insight into the geometry and electronic transitions in different absorption bands. Fig. 2 illustrates the isodensity surface plots of the three new porphyrins at the HOMO and HOMO–1 as well as LUMO and LUMO+1 energy level. The corresponding calculated energy levels are displayed in Fig. S12. As shown in Fig. 2, new porphyrin dyes present a similar planar molecule form upon varying the spacer. The HOMOs of LW7, LW8, and LW9 porphyrin dyes are delocalized through N,N–dimethylaminophenyl group and porphyrin macrocycle, while the excited electrons are shifted to the spacer and electron accepting unit (cyanoacrylic acid in LW9 for example) as observed in the LUMOs levels. This result indicates good charge separated states in these dyes upon excitation. Fig. S11 presents the energetic alignment of S^0 and S* energy levels for LW7–LW9 dyes compared to the TiO_2 conduction band (CB) and quasi–equilibrium redox potential of $[Co(bpy)_3]^{2+/3+}$ mediator. Clearly, the excited electrons can be effectively injected into the TiO_2 CB through the anchoring group.[22] With increase the electron–donating ability of the spacer, the first vertical excitation values from the calculated absorption was evaluated to be 738 nm (1.68 eV), 775 nm (1.60 eV) and 792 nm (1.56 eV) for LW7, LW8, and LW9 sensitizers, respectively. The ground state dipole moments of LW7, LW8, and LW9 sensitizers were estimated to be 11.17, 13.25 and 15.31 D, respectively. The dipole moment was increased as the spacer changed from biphenyl, bithiophene to CPDT, similar with trend of the absorption and fluorescence spectra.

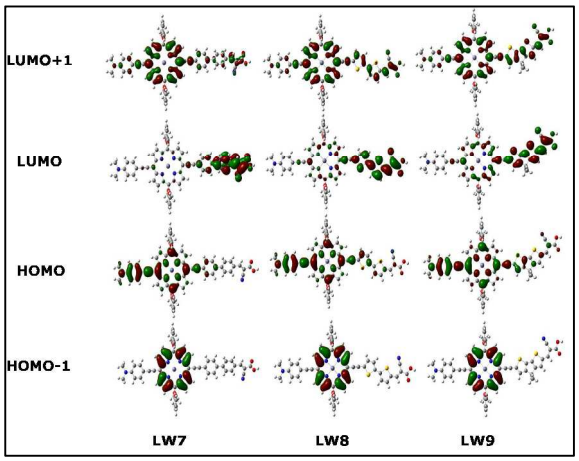

Fig. 2 Isodensity plots computed by a DFT approach of the electronic distributions of the first occupied/unoccupied orbitals of LW7, LW8, and LW9 in THF solution.

Electron injection and oxidized dye regeneration

A favourable balance between dye electron injection and dye regeneration is essential for highly efficient DSSCs.[23] In this context, TRPL and SECM were employed to characterize the electron–injection and oxidized dye regeneration processes.[24] Fig. 3 presents the fluorescence decays of LW7, LW8, and LW9 dyes in THF solution and the dye–sensitized nanocrystalline TiO_2 films filtered with cobalt complex–based electrolyte. By considering the re–convolution of instrument response function, the fluorescence lifetimes for LW7, LW8, and LW9 dyes in THF were evaluated to be 1.185, 1.073 and 1.224 ns, respectively. When adsorbed onto the TiO_2 nanoparticle surface, strong quenching of the emission for those sensitizers was observed as depicted in Fig. 3. The lifetime of the excited singlet state of LW7, LW8 and LW9 in the adsorbed state was estimated to 125.6, 71.2 and 70.0 ps. LW8 (bithiophene) and LW9 (CPDT) present absolute stronger quenching than LW7

(biphenyl), which may be explained by the twisted molecular structure of the former with thiophene derivatives as spacer (see Fig. 2). The strong quenching of the photoluminescence of LW7, LW8, and LW9 suggested that the electrons transfer from the excited dyes

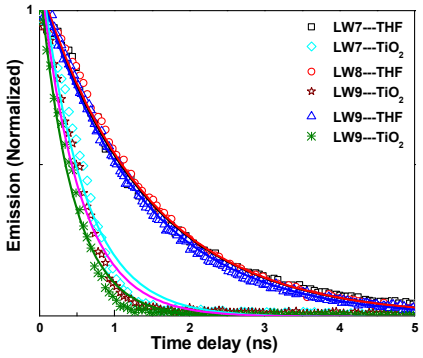

to semiconductors is absolutely fast and efficient.[25]

Fig. 3 Time-resolved photoluminescence decay traces of dye-grafted mesoporous titania film and dye in THF solvent. Excitation wavelength: 445 nm.

SECM measurements were carried out to elucidate the kinetics of interception of the different dye anions by redox couples.[26] Fig. 4a presents the normalized feedback curves for a Pt ultra-microelectrode approaching towards a FTO/TiO_2/LW9 film in electrolytes containing $[Co(bpy)_3]^{3+}$ under illumination with a red light LED (intensity 14.7×10^{-9} mol cm^{-2} s^{-1}). As shown in Fig. 4a, the interfacial charge transfer dominated the current curves when the tip approached to the sample surface. The normalized apparent heterogeneous electron transfer rate constant κ can be obtained by fitting the approach curves.[27] Based on the constant κ, the effective heterogeneous rate constant (k_{eff}, in cm s^{-1}) can be evaluated with $k_{eff}=\kappa D/rT$, where D is the diffusion coefficient for the redox couple in the electrolyte. Fig. 4b displays the calculated heterogeneous rate constants k_{eff} as a function of mediator's concentration. As can be seen in Fig. 4b, LW9 had a slight higher k_{eff} values than that of LD14 when the concentration of $[Co(bpy)_3]^{3+}$ was low, which presented similar values (about 1×10^{-3} cm s^{-1}) with that of LD14 dye when increasing $[Co(bpy)_3]^{3+}$ concentration, indicating similar apparent regeneration process for these porphyrins. Therefore, these novel porphyrins can satisfy requirements from an efficient DSSC device on fast electron injection (as shown in Fig. 3) and oxidized dye regeneration process (as shown in Fig. 4).

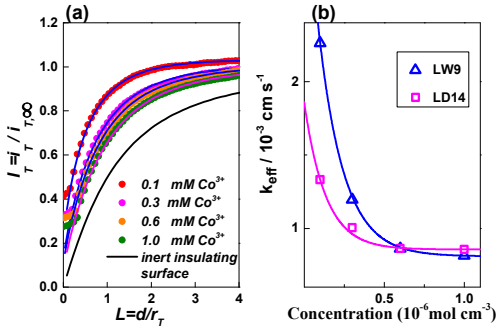

Fig. 4 (a) SECM approach curves for LW9 sensitized mesoporous TiO2 films in combination with cobalt complex electrolyte varying with concentration. (b) The comparison of effective rate (k_{eff}) for the dye regeneration reaction between the oxidized dye and $[Co(bpy)_3]^{3+}$.

Table 1. Absorption peaks, fluorescence and first porphyrin-ring redox potentials of various porphyrins (LW7, LW8, and LW9) in THF.

Dye	Absorption [a] λ_{max} (nm, $10^3/M^{-1}$ cm^{-1})	Emission [b] λ_{max} (nm)	PL [c] lifetime (ns)	E_{ox} [d] (V vs. NHE)	$E_{0\text{-}0}$ [e] (V vs. NHE)	E_{ox}-$E_{0\text{-}0}$ (eV)
LW7	461(241.4); 670(57.4)	686	1.185 (0.126)	0.703	1.832	-1.129
LW8	467(216.1) 684(81.8)	702	1.073 (0.071)	0.720	1.789	-1.069
LW9	471(147.1) 698(85.3)	725	1.22 (0.070)	0.732	1.746	-1.014
LD14[f]	457(245.4) 667(64.1)	684	1.69 (---)	0.716	1.840	-1.124

[a] Absorption and emission data were measured in THF at 25 °C; [b] Excitation wavelength for the LW7 (461 nm), the LW8 (467 nm) and LW9 (471 nm); [c] The fluorescence lifetime were measured under a laser excitation of 445 nm, in the THF solution and on the TiO_2 mesoporous film; [d] The porphyrin ring first oxidation, electrochemical measurements were performed at 25 °C with each porphyrin (0.5 mM) in THF/0.1 M TBAP/N_2, GC used as working and Pt as counter electrodes, Ag/AgCl as reference electrode, scan rate= 50 mV s^{-1}; [e] Estimated from the intersection wavelengths of the normalized UV-visible absorption and the fluorescence spectra; [f] LD14 was synthesized according to the literature.[4a]

LW7, LW8, LW9 and the reference dye LD14 were evaluated in DSSCs using $[Co(bpy)_3]^{3+/2+}$ as redox shuttle. The photovoltaic parameters, i.e., PCE, short–circuit photocurrent density (J_{SC}), the open–circuit photovoltage (V_{OC}), and fill factor (FF) of LW7, LW8, LW9 and LD14 devices are summarized in Table 2. The photocurrent–voltage curves and incident photon to current efficiency (IPCE) spectra are displayed in Fig. 5. The device of LW9 (CPDT) exhibited a J_{SC} of 11.47±0.16 mA cm^{-2}, a V_{OC} of 738±8 mV, a FF of 0.76±0.02, giving an overall PCE of 6.50±0.06%, while LW7 (biphenyl) was 9.58±0.34 mA cm^{-2}, 802±4 mV, 0.78±0.03, 6.02±0.11% and LW8 (bithiophene) was 10.37±0.24 mA cm^{-2}, 788±6 mV, 0.76±0.02, 6.32±0.08%. The J_{SC} of LW9 device was higher than LW7 and LW8 devices. Under similar conditions, the reference porphyrin LD14 gave an efficiency of 7.93%. The dramatically decrease in V_{OC} of LW9 devices relative to the others may be account of serious interfacial charge recombination, which will be discussed in the next part. As shown in Fig. 5b, LW9 device possessed a broadened light–harvesting area up to 800 nm and aroused shoulder in 500–550 nm, explaining its higher J_{SC} comparing to LW7 and LW8 devices. It was also observed that the onset wavelengths of photocurrent response was stepwise extended from LW7, LW8 to LW9, which were in general agreement with the electronic absorptions of dye–sensitized 2.3–μm–thick titania films (Fig. S8).

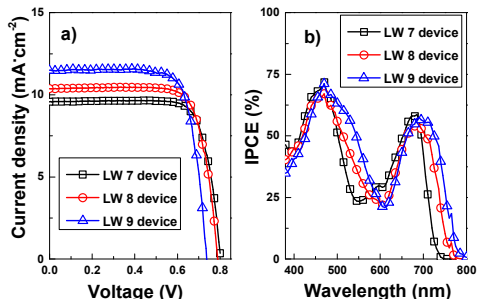

Fig. 5 a) *J–V* curves of and the DSSC devices based on LW7, LW8 and LW9 porphyrins measured under simulated AM 1.5G full sunlight, and b) IPCE spectra of LW7, LW8 and LW9 devices. The cells were measured with a mask (area= 0.09 cm^{-2}).

Table 1. Photovoltaic parameters [a] of porphyrins sensitized solar cells with $[Co(bpy)_3]^{2+/3+}$ redox couple (AM 1.5G 96.5 mW cm^{-2}). The cells were measured using a mask (area= 0.09 cm^{-2}).

device	J_{SC} (mA cm^{-2})	V_{OC} (mV)	*FF*	PCE (%)
LW7	9.58±0.34	802±4	0.78±0.03	6.02±0.11
LW8	10.37±0.24	788±6	0.76±0.02	6.32±0.08
LW9	11.47±0.16	738±8	0.76±0.02	6.50±0.06
LD14	13.23±0.10	810±6	0.73±0.01	7.93±0.02

[a] The uncertainties represent the standard deviations of the measurements. The photovoltaic parameters are averaged values obtained from analysis of the J–V curves of the identical working electrodes for three devices, fabricated and characterized under the same experimental conditions.

TPD and charge extraction measurements were employed to get insight into the details of electron recombination dynamics between the photoinjected electrons at the TiO_2 and the oxidized electrolyte in LW7, LW8, LW9 devices.[28] The variations of V_{OC} may be ascribed to a shift of the TiO_2 conduction band edge bending with respect to the electrolyte potential and/or differences in the e^-–TiO_2/electrolyte$^+$ recombination reaction.[29] According to the literature,[5] chemical capacitance ($C\mu$) provides information about the shift of conduction band edge of TiO_2 and the distribution of trap states. As presented in Fig. 6a, LW7 and LW8 devices showed lower $C\mu$ compared to LW9 at a given V_{OC}, indicating a trend of conduction band bending of LW7>LW8>LW9. Comparing to the LW7 dye using bithiophene as spacer, CPDT in the LW9 dye leads to a negative shift (versus NHE) of the conduction band edge of TiO_2 of about 40 mV. Similar phenomenon was found by Gao *et al.*, sowing that a negative shift of the conduction band bending of 50 mV was caused by employing a CPDT instead of the spacer in organic dyes.[30] The relationship of electron lifetimes as a function of V_{OC} was given in Fig. 6b, affording insight into the electron recombination occurring at the TiO_2/electrolyte interface. The LW9 device presented a shorter lifetime comparing to LW7 and LW8 devices, implying a faster recombination reaction on the dye-sensitized TiO_2/electrolyte interface. As we know, a faster electron recombination is always followed a negative shift (versus NHE) of the conduction band edge of TiO_2. Therefore, the observed drop of photovoltage of LW9 comparing to that of LW8 could be principally due to a negative shift of the conduction band edge of TiO_2.

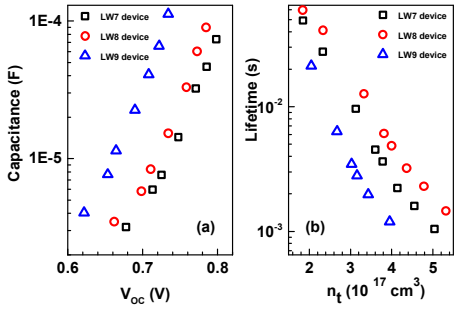

Fig. 6 Transient photovoltage decay and charge extraction measurements of LW7, LW8, and LW9 based DSSC devices. a) Comparisons of chemical capacitance at a certain open–circuit photovoltage; b) Comparisons of electron lifetime at a given electron density.

Conclusions

This work presents a method to broaden the light-harvesting area for porphyrin sensitizer with D–π–D–A approach. Porphyrin (LW9) with cyclopenta[1,2–b:5,4–b′]dithiophene as spacer between the porphyrin chromophore and cyanoacetic acid exhibited intensively red-shifted absorption spectra, together with obvious splitting of the B band at 520 nm. Therefore, LW9 offers a light–harvesting ability through visible spectrum to near–IR region. To investigate the influence from spacer, biphenyls, bithiophene conjugated porphyrin were also synthesized and investigated. These porphyrins presented stepwise red–shift of absorption spectra and consistent decreased energy gap, which was quite consistent with increase of electron-donating ability of spacer. PCE of 6.0%, 6.3% and 6.5% with $[Co(bpy)_3]^{2+/3+}$ redox couple was achieved for LW7, LW8, and LW9 dyes, respectively. A higher J_{SC} of LW9 device was ascribed to the broadened light-harvesting area. However, the fast interfacial charge recombination process and TiO_2 conduction band bending caused a significant drop of V_{OC}. The low PCE of these devices could be due to the improper molecular structure of the dye. To increase the V_{OC} and efficiency of DSSCs, further optimization of the molecular structure based on LW9 porphyrin is on–going.

Acknowledgements

Financial support from the NSFC (21103057, 21161160445, 21173091), the Innovation Fund of Innovation Institute (HUST CXY13Q009) and the CME with the Program of New Century Excellent Talents in University (NCET–10–0416), are gratefully acknowledged. The authors thank Chong Li and the Analytical and Testing Centre at the HUST for performing the characterization of various samples. Y.S. and M.W. thank the Carl von Ossietzky University of Oldenburg for the support as visiting scientist.

Notes and references

[a] *Michael Grätzel Center for Mesoscopic Solar Cells, Wuhan National Laboratory for Optoelectronics, School of Optical and Electronic Information，Huazhong University of Science and Technology, 1037 Luoyu Road, Wuhan 430074 (P. R. China)，Fax: (+) 86 27 87792225，E-mail: mingkui.wang@mail.hust.edu.cn, ciac_sheny@mail.hust.edu.cn*

[b] *College of Materials Science & Engineering, Wuhan Textile University, FangZhi Road, 430073, Wuhan, P. R. China, E-mail: xujie0@mail.ustc.edu.cn*

[c] *Department of Materials Engineering, Monash University Melbourne, Victoria, 3800, Australia.*

Electronic Supplementary Information (ESI) available: [details of any supplementary information available should be included here]. See DOI: 10.1039/b000000x/

1 a) B. O' Regan, M. Grätzel, *Nature*, 1991, **353**, 737–740; b) S. Kazim, M. K. Nazeeruddin, M. Grätzel, S. Ahmad, *Angew. Chem., Int. Ed.,* 2014, **53**, 2812–2824; c) P. K. Nayak, D. Cahen, *Adv. Mater.*, 2014, **26**, 1622–1628.

2 a) C. Y. Chen, M. K. Wang, J. Y. Li, N. Pootrakulchote, L. Alibabaei, C. H. Ngocle, J. D. Decoppet, J. H. Tsai, C. Grätzel, C. G. Wu, S. M. Zakeeruddin, M. Grätzel, *ACS Nano,* 2009, **3**, 3103–3109; b) K. Cao, J. F. Lu, J. Cui, Y. Shen, W. Chen, G. Alemu, Z. Wang, H. L. Yuan, J. Xu, M. K. Wang, Y. B. Cheng, *J. Mater. Chem. A,* 2014, **2**, 4945–4953.

3 a) A. Mishra, M. K. R. Fischer, P. Bauerle, *Angew. Chem., Int. Ed.*, 2009, **48**, 2474–2499; b) K. Cao, M. K. Wang, *Front. Optoelectron.* 2013, **6**, 373–385.

4 a) Y. C. Chang, C. L. Wang, T. Y. Pan, S. H. Hong, C. M. Lan, H. H. Kuo, C. F. Lo, H. Y. Hsu, C. Y. Lin, E. W. G. Diau, *Chem. Comm.* 2011, **47**, 8910–8912; b) C. L. Wang, C. M. Lan, S. H. Hong, Y. F. Wang, T. Y. Pan, C. W. Chang, H. H. Kuo, M. Y. Kuo, E. W. G. Diau, C. Y. Lin, *Energy. Environ. Sci.*, 2012, **5**, 6933–6940; c) M. J. Griffith, K. Sunahara, P. Wagner, K. Wagner, G. G. Wallace, D. L. Officer, A. Furube, R. Katoh, S. Mori, A. J. Mozer, *Chem. Comm.,* 2012, **48**, 4145–4162; d) Y. Z. Liu, H. Lin, J. T. Dy, K. Tamaki, J. Nakazaki, D. Nakayama, S. Uchida, T. Kubo, H. Segawa, *Chem. Comm.*, 2011, **47**, 4010–4012; C. W. Lee, H. P. Lu, C. M. Lan, Y. L. Huang, Y. R. Liang, W. N. Yen, Y. C. Liu, Y. S. Lin, E. W. G. Diau, C. Y. Yeh, *Chem. Eur. J.,* 2009, **15**, 1403–1412; e) W. M. Campbell, K. W. Jolley, P. Wagner, K. Wagner, P. J. Walsh, K. C. Gordon, L. Schmidt-Mende, M. K. Nazeeruddin, Q. Wang, M. Grätzel, D. L. Officer, *J. Phys. Chem. C,* 2007, **111**, 11760-11762; f) L. L. Li, E. W. G. Diau, *Chem. Soc. Rev.,* 2013, **42**, 291–304; g) C. F. Lo, S. J. Hsu, C. L. Wang, Y. H. Cheng, H. P. Lu, E. W. G. Diau, C. Y. Lin, *J. Phys. Chem. C*, 2010, **114**, 12018–12023.

5 a) A. Yella, H. W. Lee, H. N. Tsao, C. Y. Yi, A. K. Chandiran, M. K. Nazeeruddin, E. W. G. Diau, C. Y. Yeh, S. M. Zakeeruddin, M. Grätzel, *Science*, 2011, **334**, 629–634; b) M. Mathew, A. Yella, P.; R. Humphry-Baker, Basile F.E.Curchod, N. Ashari-Astani, I. Tavernelli, U. Rothlisberger, M. K. Nazeeruddin, M. Grätzel, *Nat. Chem.*, 2014, **6**, 242–247.

6 a) A. Yella, C. L. Mai, S. M. Zakeeruddin, S. N. Chang, C. H. Hsieh, C. Y. Yeh, M. Grätzel, *Angew. Chem., Int. Ed.*, 2014, **126**, 3017–3021; b) C. Y. Yi, F. Giordano, N. Cevey-Ha, H. N. Tsao, S. M. Zakeeruddin, M. Grätzel, *ChemSusChem*, 2014, 7, 1107–1113; c) W. Julien, F. Ludovic, M. Frederic, S. Marjorie, B. Errol, P. Yann, J. Denis, O. Fabrice, *ChemSusChem*, 2012, **5**, 1568–1577.

7 J. Luo, M. F. Xu, R. Z. Li, K. W. Huang, C. Y. Jiang, Q. B. Qi, W. D. Zeng, J. Zhang, C. Y. Chi, P. Wang, J. S. Wu, *J. Am. Chem. Soc.*, 2014, **136**, 265–272.

8 a) K. Kurotobi, Y. Toude, K. Kawamoto, Y. Fujimori, S. Ito, P. Chabera, V. Sundstrçm, H. Imahori, *Chem. Eur. J.*, 2013, **19**, 17075–17081; b) G. Carlo, A. Biroli, M. Pizzotti, F. Tessore, V. Trifiletti, R. Ruffo, A. Abbotto, A. Amat, F. De Angelis, P. Mussini, *Chem. Eur. J.*, 2013, **19**, 10723–10740; c) H. Imahori, T. Umeyama, S. Ito, *Acc. Chem. Res.*, 2009, **42**, 1809–1818; d) C. L. Wang, J.Y. Hu, C. H. Wu, H. H. Kuo, Y. C. Chang, Z. J. Lan,H. P. Wu, E. W. G. Diau，C. Y. Lin, *Energy. Environ. Sci.,* 2014, **7**, 1392–1396; e) M. D. Zhang, Z. Y. Zhang, Z. Q. Bao, Z. M. Ju, X. Y. Wang, H. G. Zheng, J. Ma, X. F. Zhou, *J. Mater. Chem. A*, 2014, **2**, 14883-14889; f) M. Sreenivasu, A. Suzuki, M. Adachi, C. Kumar, B. Srikanth, S. Rajendar, D. Rambabu, R. Kumar, P. Mallesham, N. Bhaskar Rao, M Kumar, P. Reddy, *Chem. Eur. J.*, 2014, DOI: 10.1002/chem.201403660.

9 Y. Liu, N. Xiang, X. Feng, P. Shen, W. Zhou, C. Weng, B. Zhao, S. Tan, *Chem. Comm.,* 2009, **45**, 2499–2501.

10 S. Mathew, H. Iijima, Y. Toude, T. Umeyama, Y. Matano, S. Ito, N. V. Tkachenko, H. Lemmetyinen, H. Imahori, *J. Phys. Chem. C*, 2011, **115**, 14415–14424.

11 C. J. Jiao, N. N. Zu, K. W. Huang, P. Wang, J. S. Wu, *Org. Lett.* 2011, **13**, 3652–3655.

12 C. L. Wang, J. Y. Hu, C. H. Wu, H. H. Kuo, Y. C. Chang, Z. J. Lan, H. P. Wu, E. W. G Diau, C. Y. Lin, *Energy. Environ. Sci.* 2014**,** **7**, 1392–1396.

13 J. M. Ball, N. K. S. Davis, J. D. Wilkinson, J. Kirkpatrick, J. Teuscher, R. Gunning, H. L. Anderson, H. J. Snaith, *RSC Adv.*, **2012**, 2, 6846–6853.

14 a) L. Favereau, J. Warnan, F. B. Anne, Y. Pellegrin, E. Blart, D. Jacquemin, F. Odobel, *J. Mater. Chem.* A, 2013, **1**, 7572–7575; b) C. Y. Lee, J. T. Hupp, *Langmuir*, 2010, **26**, 3760–3765.

15 a) J. F. Lu, X. B. Xu, K. Cao, J. Cui, Y. B. Zhang, Y. Shen, X. B. Shi, Liao, L. S.; Y. B. Cheng, M. K. Wang, *J. Mater. Chem. A*, 2013, **1**, 10008–10015; b) J. F. Lu, B. Y. Zhang, H. L. Yuan, X. B. Xu, K. Cao, J. Cui, S. S. Liu, Y. Shen, Y. B. Cheng, M. K. Wang, *J. Phys. Chem. C*, 2014, **118**, 14739–14748; c) J. F. Lu, S. S. Liu, H. Li, Y. Shen, J. Xu, M. K. Wang, *J. Mater. Chem. A*, 2014, DOI: 10.1039/C4TA03435J.

16 a) W. H. Nguyen, C. D. Bailie, J. Burschka, T. Moehl, M. Grätzel, M. D. McGehee, A. Sellinger, *Chem. Mater.*, 2013, **25**, 1519–1525; b) L. Polander, A. Yella, J. Teuscher, R. Humphry-Baker, B. Curchod, N. Astani, P. Gao, J. Moser, I. Tayernelli, U.; M. Grätzel, et al., *Chem. Mater.*, 2013, **25**, 2642–2648; c) A. Yella, R. Humphry-Baker, B. Curchod, N. Astani, J. Teuscher, L. Polander, S. Mathew, J. Moser, I. Tavernelli, U. Rothlisberger, et al., *Chem. Mater.*, 2013, **25**, 2733–2739; d) H. X. Zhou, L. Q. Yang, W. You, *Macromolecules*, 2012, **45**, 607–632.

17 J. S. Lindsey, *Acc. Chem. Res.*, 2010, **43**, 300–311.

18 J. F. Lu, X. B. Xu. Z. H. Li, K. Cao, J. Cui, Y. B. Zhang, Y. Shen, Y. Li, J. Zhu, S. Y. Dai, et al., *Chem. Asian J.*, 2013, **8**, 956–962.

19 a) J. Rochford, D. Chu, A. Hagfelt, E. Galoppini, *J. Am. Chem. Soc.*, 2007, **129**, 4655–4665; b) M. Gouterman, *J. Chem. Phys.*, 1959, **30**, 1139–1161.

20 a) H. J. Snaith, *Adv. Funct. Mater.*, 2010, **20**, 13–19; b) A. Hagfeldt, G. Boschloo, L. C. Sun, L. Kloo, H. Pettersson, *Chem. Rev.* 2010, **110**, 6595–6663.

21 a) M. K. Wang, C. Grätzel, S. Zakeeruddin, M. Grätzel, *Energy Environ. Sci.*, 2012, **5**, 9394–9405; b) J. F. Lu, J. Bai, X. B. Xu, Z. H. Li, K. Cao, J. Cui, M. K. Wang, *Chin. Sci. Bull.*, 2012, **57**, 4131–4142.

22 a) H. Imahori, S. Kang, H. Hayashi, M. Haruta, H. Kurata, S. Isoda, S. E. Canton, Y. Infahsaeng, A. Kathiravan, T. Pascher, et al. *J. Phys. Chem. A*, 2011, **115**, 3679–3690; b) S. Ye, A. Kathiravan, H. Hayashi, Y. J. Tong, Y. Infahsaeng, P. Chabera, T. Pascher, A. P. Yartsev, S. Isoda, H. Imahori, et al. *J. Phys. Chem. C*, 2013, **117**, 6066–6080; L. P. Cai, H. N. Tsao, W. Zhang, L. Wang, Z. S. Xue, M. Grätzel, B. Liu, *Adv. Energy Mater.*, 2013, **3**, 200–205.

23 B. E. Hardin, H. J. Snaith, M. D. McGehee, *Nat. Photonics*, 2012, **6**, 162–169.

24 a) S. E. Koops, B. O'Regan, P. R. F. Barnes, J. R. Durrant, *J. Am. Chem. Soc.*, 2009, **131**, 4808–4818; b) X. B. Xu, B. Y. Zhang, J. Cui, D. Xiong, Y. Shen, W. Chen, L. Sun, W. Cheng, M. K. Wang, *Nanoscale*, 2013, **5**, 7963–7969.

25 a) X. D. Yang, S. F. Zhang, K. Zhang, J. Liu, C. J. Qin, H. Chen, A. Islama, L. Y. Han, *Energy. Environ. Sci.,* 2013, **6**, 3637–3645; b) Y. Chang, H. Wu, N. Reddy, H. Lee, H. Lu, C. Yeh, E. W. G. Diau, *Phys. Chem. Chem. Phys.*, 2013, **15**, 4651–4655.

26 Y. Shen, K. Nonomura, D. Schlettwein, C. Zhao, G. Wittstock, *Chem. Eur. J.*, 2006, **12**, 5832–5839.

27 B. Y. Zhang, X. B. Xu. X. F. Zhang, D. K. Huang, S. H. Li, Y. B. Zhang, F. Zhan, M. Z. Deng, Y. H. He, W. Chen, Y. Shen, M. K. Wang, *ChemPhysChem*, 2014, **15**, 1182–1189.

28 a) L. L. Li, Y. C. Chang, H. P. Wu, E. W. G. Diau, *Int. Rev. Phys. Chem.* **2012**, 31, 420–467; b) J. Bisquert, A. Zaban, M. Greenshtein, I. Mora-Sero, *J. Am. Chem. Soc.*, 2004, **126**, 13550–13559.

29 a) M. K. Wang, P. Chen, R. Humphry-Baker, S. M. Zakeeruddin, M. Grätzel, *ChemPhysChem*, 2009, **10**, 290–299; b) A. Reynal, A. Forneli, E. Martinez-Ferrero, A. Sanchez-Diaz, A. Vidal-Ferran, B. O'Regan, E. Palomares, *J. Am. Chem. Soc.*, 2008, **130**, 13558–13567.

30 P. Gao, H. N. Tsao, C. Y. Yi, M. Grätzel, M. K. Nazeeruddin, *Adv. Energy Mater.*, 2014, 4, DOI: 10.1002/aenm.201301485.

